Vacuum 205 (2022) 111485

Contents lists available at ScienceDirect

Vacuum

journal homepage: www.elsevier.com/locate/vacuum

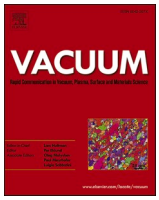

Improved photoenergy properties of low-emissivity coatings deposited by sputtering with an ion gun treatment

E. Carretero [a,*], A. Cueva [a], J. Preciado-Garbayo [b], P. Sevillano [a]

[a] Departamento de Física Aplicada, Universidad de Zaragoza, C/Pedro Cerbuna, 12, 50009, Zaragoza, Spain
[b] Departamento de Ingeniería Electrónica y Comunicaciones, Universidad de Zaragoza, C/ Maria de Luna, 1, Zaragoza, 50018, Spain

ARTICLE INFO

Keywords:
Sputtering
Thin films
Low-emissivity coatings
Ion treatment
Optical properties

ABSTRACT

This work studies the effect of ion treatment on low-emissivity (low-e) coatings deposited by magnetron sputtering. Specifically, we have investigated the application of an ion treatment in the dielectric layer before deposition of a layer of silver. This reduces layer roughness which means the silver layer can be deposited with enhanced characteristics. We have also evaluated the etching rate on the SnO_x layer due to the ion treatment on already deposit coatings of equal thicknesses. Subsequently, we studied the effects on the coating's photoenergy properties. For equivalent coatings, we found that those treated with ions were more transparent in the visible region, more reflective, and had a lower emissivity, which are essential requirements for low-e coatings applied in architectural glass.

1. Introduction

Glazing plays a crucial role in several industries including automotive, locomotive and construction. Glazed areas act as the interface that enables visual communication between the inside and outside worlds. However, any glazed areas must feature specific energy-insulating properties, so that they also offer greater comfort and habitability, while minimizing energy consumption.

The main component of modern glazing is soda-lime silicate glass, which offers excellent transparency and high chemical and environmental stability. Nevertheless, one of its main disadvantages is poor thermal insulation. This drawback has been resolved adequately using double glazing configurations plus selective low-emissivity and solar control coatings that reduce both energy losses in winter and solar gain in summer [1–4].

The development of low-emissivity glasses with solar control properties derives from the basic structure of substrate/MeO_x/Ag/metallic barrier/MeO_x [5], that is, a silver layer sandwiched between two transparent oxide layers. The silver layer provides low emissivity and is the ideal material for this task because it has high reflectivity in the mid- and far-infrared regions [6], while reducing solar transmittance in the near-infrared region. The two transparent metal oxide layers act as visible anti-reflection layers, thus achieving a high transparency [7]. Furthermore, a very thin metallic barrier layer (2–3 nm) must be deposited on top of the silver layer to prevent it from oxidizing when depositing the subsequent MeO_x layer [8]. Although the use of these coatings is commonplace, they do not have much visible light/infrared selectivity; they present 60% transmittance at 800 nm, which equates to limited solar control properties. To improve this selectivity, and therefore its solar control properties, more complex coatings based on a double Ag structure of substrate/MeO_x/Ag/metallic barrier/MeO_x/-Ag/metallic barrier/MeO_x are used with more selective spectral properties [9,10]. This type of structural arrangement has been widely exploited by glass manufacturers to develop various products with these properties [11].

Better emissivity can be achieved by reducing the roughness of the dielectric layers. This means the silver layers will acquire a better crystalline structure when coated after the ion gun treatment, thus reducing their electrical resistance and improving the emissivity of the coating [12,13].

Physical vapor deposition (PVD) is the most common technique for obtaining low-emissivity coatings [14]. It consists of ion bombardment of a material followed by its evaporation deposition onto the surface of the substrate [15]. The present works looked at the properties of different low-emissivity coatings deposited by PVD. The substrate was pretreated with an ion gun system before depositing the silver layers. We applied argon ion bombardment to the dielectric layer before the silver layer to achieve a smooth dielectric surface. We found that the silver

* Corresponding author.
E-mail address: ecarre@unizar.es (E. Carretero).

https://doi.org/10.1016/j.vacuum.2022.111485
Received 3 June 2022; Received in revised form 2 September 2022; Accepted 3 September 2022
Available online 11 September 2022

grew in a more crystalline structure when deposited on dielectric layers previously treated with an ion gun, which resulted in lower emissivity throughout the whole structure [16].

Typically, SnO_2 has been used for the metal oxide layer, mainly because its optical properties are suitable for this application and also thanks to its high deposition rate compared to other metal oxides. SnO_2 is the most used material in industrial applications because its high deposition rate means it requires a shorter cycle time in the production line [6,8,17,18]. On the other hand, there are other metal oxides such as ZnO, AZO (aluminum–zinc oxide), ZrO_2, TiO_2, and so on [19–24] which also have suitable optical properties for this type of coating, but they are used to a lesser extent because of more complicated processing and lower deposition rates. However, some of these metal oxides have a more suitable microstructure for the deposition of the Ag layer and consequently offer better photoenergy properties than those achieved with SnO_2 [13,21,25]. Regarding the optical properties, SnO_2 presents optimal values for its application in low emissive coatings, however, several attempts have been made to improve the properties of the coatings with new treatments or techniques [26,27]. In this work we aimed to improve the surface of the SnO_x layers by means of an ion gun treatment to ultimately obtain coatings with improved photoenergy properties, while also retaining the productive advantage associated with the high deposition rate of SnO_x by means of the sputtering technique.

2. Experimental

2.1. Experimental setup

All the coatings being studied were deposited in a semi-industrial (inline) high vacuum system using magnetron sputtering (see Figure S1(a-b) Supplementary Material). The deposition system featured DC pulsed power supplies and 600 mm × 100 mm rectangular targets. Mass flow controllers (MFC) were used to control the amount of gas injected into the vacuum chamber. While the discharge was taking place, that is, while the layer was being deposited, the substrate carrier moved through the process chamber at a constant speed, so each point on the substrate received exactly the same exposure to the deposition process, producing an uniform coating with a homogeneous thickness. As such, the thickness deposited on the substrate was inversely proportional to the speed of the carrier. The system also included an ion gun to help produce a cleaner substrate prior to deposition and therefore better adhesion of the layers [28]. In the deposition system there is a cryo pump in order to reduce the residual water vapor. We used low-iron sodium-calcium glass substrates (Pilkington Optiwhite™), measuring 100 mm × 100 mm and 4 mm thick, previously cleaned with a special glass detergent (ACEDET 5509).

The linear ion gun is approximately 600 mm long. An acceleration voltage of 2 kV was applied and a flow of 0.84 Pa m^3 s^{-1} of Ar was introduced into the vacuum chamber during bombardment. The dose applied in each case was inversely proportional to the speed of the carrier. The ion beam was pointed perpendicularly on the sample. By doing that, all the points of the sample received the same ion dose with the same angle of incidence due to the inline process.

Layer thicknesses were measured with a DektakXT® mechanical profilometer, which has a precision of approximately 1 nm.

X-ray diffraction data were collected using a Rigaku D/Max, Ru300 diffractometer, equipped with a rotating Cu anode. The diffractometer was operated at 40 kV and 80 mA using a graphite monochromator to select Cu K-alpha radiation. The measurement parameters were from $2\theta = 20^\circ$ to 80° with step $= 0.03^\circ$ and t = 1 s/step. Phase determination was based on the JCPDS–International Center for Diffraction Data 2000 database.

Structural characterization and elemental mapping was performed using Transmission Electron Microscopy TITAN (FEI Company) with EDS detector "EDS Oxford Instruments Ultim Max TLE 100". Surface roughness measurements of SnO_x films was performed using Atomic Force Microscopy (AFM) Dimension Icon (Bruker).

Optical measurements were made with a UV–Vis/NIR spectrophotometer designed and built by the Photonic Technologies Group at the University of Zaragoza. The spectrophotometer can perform transmission and specular reflection measurements across the entire range of the solar spectrum, from 300 to 2500 nm, with an angle of incidence of 8°.

We used the following equations to calculate the photoenergy factors that characterize low-emissivity and solar control coatings:

$$T_{VIS} = \frac{\int_{380nm}^{780nm} T(\lambda)V(\lambda)D_{65}(\lambda)d\lambda}{\int_{380nm}^{780nm} V(\lambda)D_{65}(\lambda)d\lambda} \quad (1)$$

$$T_{SOLAR} = \frac{\int_{300nm}^{2500nm} T(\lambda)S(\lambda)d\lambda}{\int_{300nm}^{2500nm} S(\lambda)d\lambda} \quad (2)$$

where $T(\lambda)$ is the spectral transmittance factor (measured with the spectrophotometer), $V(\lambda)$ is the normalized human eye spectral sensitivity curve, $D_{65}(\lambda)$ is the standard illuminator, and $S(\lambda)$ is the solar spectrum. Similarly, analogous values can be calculated for reflectance.

Conductivity was measured via two methods: a 4-point probing method using a Jandel RM3000 m and the sheet resistance using a NAGY SRM-12 instrument. Sample emissivity was calculated from the following equation [29]:

$$\varepsilon_n = 0.0106 \cdot R_{\square} \quad (3)$$

where ε_n is the emissivity normal to the surface of the sample and $R_{\square}$ stands for the sheet resistance.

2.2. Samples

The layers studied in this work consist of low-emissivity structures with dielectric layers of tin oxide. The base pressure of the deposition system was $7 \cdot 10^{-7}$ mbar. The working pressure was between 1 and $2 \cdot 10^{-3}$ mbar, depending on the layer (a flow of 3.38 Pa m^3 s^{-1} is equivalent to a pressure of approximately $1 \cdot 10^{-3}$ mbar). Table 1 shows the deposition parameters for each layer. The oxygen flow for SnO_x deposition was calibrated ensuring that the process worked in reactive mode (see calibration curve in Figure S2 of the Supplementary Material).

Low-emissivity coatings with structures such as SnO_x/Ag/Ti/SnO_x and SnO_x/Ag/Ti/SnO_x/Ag/Ti/SnO_x were deposited using the same high vacuum deposition system. Layer thickness could be controlled by adjusting the speed of the substrate holder. The ion gun had the effect of etching the layer deposited previously. Therefore, to obtain samples with similar optical properties, the layers deposited were slightly thicker than required to compensate for the etching. Table 2 shows the composition of the layers for six different samples, four of them with a

Table 1
Deposition parameters for each material and the ion gun.

Material	Power (W)	Power density (W/cm^2)	Ar flow (Pa·m^3·s^{-1})	O_2 flow (Pa·m^3·s^{-1})
SnO_x	2000	3.33	2.53	3.04
Ag	500	0.83	5.06	0
Ti	800	1.33	3.38	0
Ion gun	2 kV		0.84	0

Table 2
Composition and thickness of each layer deposited. Negative values in thickness indicates the etching thickness by ion treatment.

Material	Layer No.	Sample 1		Sample 2		Sample 3		Sample 4		Sample 5		Sample 6	
		Thickness (nm)		Thickness (nm)		Thickness (nm)		Thickness (nm)		Thickness (nm)		Thickness (nm)	
		Ref	Ion	Ref	Ion	Ref	Ion	Ref	Ion	Ref	Ion	Ref	Ion
Substrate													
SnO_x	1	29	44	24	39	30	60	15	30	29	44	30	45
Ion gun		–	−15	–	−15	–	−30	–	−15	–	−15	–	−15
Ag	2	10	10	15	15	20	20	27	27	9	9	7	7
Ti	3	3	3	3	3	3	3	3	3	3	3	3	3
SnO_x	4	45	45	49	49	8	8	53	53	77	92	78	93
Ion gun		–	–	–	–	–	–	–	–	–	−15	–	−15
Ag	5	–	–	–	–	–	–	–	–	14	14	19	19
Ti	6	–	–	–	–	–	–	–	–	3	3	3	3
SnO_x	7	–	–	–	–	–	–	–	–	34	34	32	32

single layer of silver (with different thicknesses) and two of them with two layers of silver. The ion gun was always applied before depositing a layer of silver and Table 2 shows the thickness eroded at the applied dose (0.420 cm/s in all samples except 0.210 cm/s in sample 3). We prepared at least two specimens of each sample; a reference specimen (Ref) without applying the ion treatment and the specimen with the ion treatment (Ion). For Samples 1 and 5, we also studied the effect of ion dose (Tables 3 and 4). Note that the most external layer of SnO_x was thinner in Sample 3 (less than the optimal optical thickness) so the crystallinity of the silver layer could be studied in more detail by means of X-ray diffraction.

3. Results and discussion

3.1. Calibration of etching based on ion dose

The first step is to characterize the etching on the SnO_x layer due to the application of the ion gun. This is crucial because the optical properties of the coating are heavily dependent on the thickness of the SnO_x layer. This impact is especially pronounced on the transmittance and reflectance in the visible range, because SnO_x layer thickness can significantly modify the interference due to the multiple reflections in the multilayer. For this reason, we deposited a 100 nm layer of SnO_x on different samples under the same conditions and at different doses of exposure to the ion gun (inversely proportional to the speed of the substrate holder); the etching as a function of ion dose is shown in Fig. 1. As expected, the etching effect increased with the ion dose. However, it did not increase linearly, because the ionic bombardment compacted the remaining layer, so after a certain amount of bombardment, the resulting layer was more resistant to etching. This level of etching was taken as a reference in Tables 2-4 when determining how much extra thickness to deposit in the SnO_x layers before applying the ion gun. The result was SnO_x layers with an ideal thickness in terms of their optical properties and coatings comparable to the reference samples.

Table 3
Sample 1 layer thicknesses at different ion doses.

Sample 1	Sample 1.Ref	Sample 1.1	Sample 1.2	Sample 1.3	Sample 1.4	Sample 1.5
Carrier speed	—	1.680 cm/s	0.840 cm/s	0.420 cm/s	0.210 cm/s	0.105 cm/s
Substrate						
SnO_x	29	34	39	44	59	69
Ion gun	—	−5	−10	−15	−30	−40
Ag	10	10	10	10	10	10
Ti	3	3	3	3	3	3
SnO_x	45	45	45	45	45	45

Table 4
Sample 5 layer thicknesses at different ion doses.

Sample 5	Sample 5.Ref	Sample 5.1	Sample 5.2	Sample 5.3	Sample 5.4	Sample 5.5
Carrier speed	—	1.680 cm/s	0.840 cm/s	0.420 cm/s	0.210 cm/s	0.105 cm/s
Substrate						
SnO_x	29	34	39	44	59	69
Ion gun	—	−5	−10	−15	−30	−40
Ag	10	10	10	10	10	10
Ti	3	3	3	3	3	3
SnO_x	77	82	87	92	107	117
Ion gun	—	−5	−10	−15	−30	−40
Ag	14	14	14	14	14	14
Ti	3	3	3	3	3	3
SnO_x	34	34	34	34	34	34

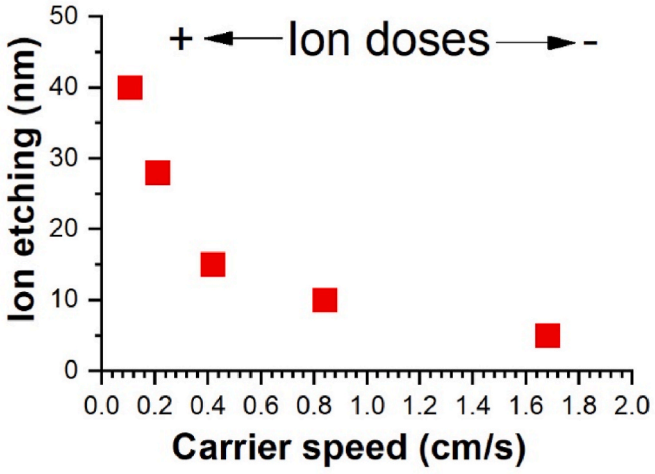

Fig. 1. Ion etching of SnO_x as a function of ion dose.

3.2. AFM and XRD

We studied the surface morphology of a 100 nm layer of SnO_x by AFM (Top-view photos performed by FESEM are also shown in Figure S3 of the Supplementary Material). Fig. 2 shows the difference in the surface morphology of four SnO_x samples. First sample had no treatment (Fig. 2a) and the measured roughness is 1.0 nm (Table 5). The second sample had ion treatment at a speed of 0.840 cm/s (Fig. 2b) and it can be seen that the surface morphology has been modified obtaining a similar roughness of 1.0 nm but with smaller diameter bulges. Sample 3 had ion treatment at a speed of 0.420 cm/s (Fig. 2c), in this case the roughness is reduced to 0.7 nm preserving the small bulges size. The last sample had

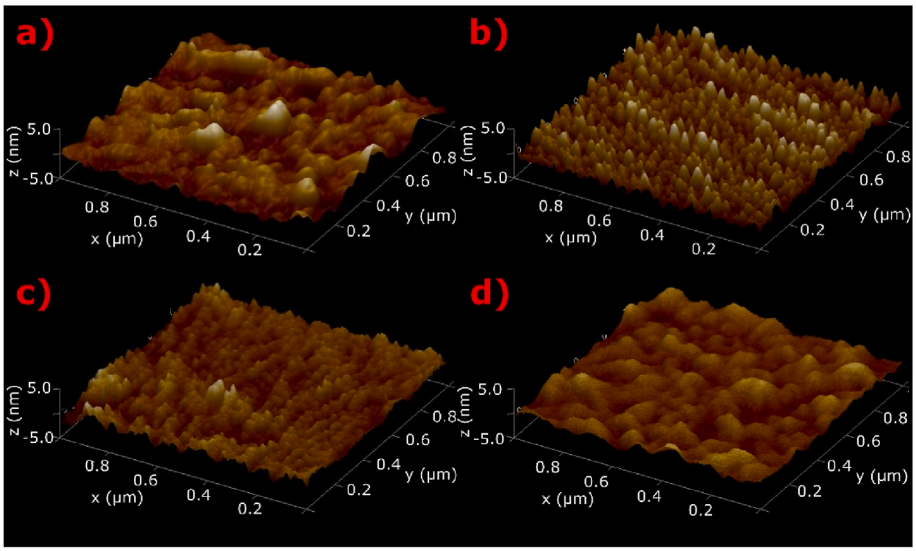

Fig. 2. AFM images of the "top surface" of a 100 nm layer of SnO_x: a) as deposited, b) after ion gun treatment at 0.840 cm/s, c) at 0.420 cm/s and d) at 0.105 cm/s.

Table 5
Roughness as a function of ion dose.

Carrier speed (cm/s)	Rq (nm)
No ion	1.0
0.840	1.0
0.420	0.7
0.105	0.7

ion treatment at a speed of 0.105 cm/s (Fig. 2d) and the roughness obtained is 0.7 nm but for this case the diameter of bulges is similar to the sample that had no ion treatment. This means the silver layer deposited over the SnO_x layer after the treatment is more uniform when moderate ion doses are applied, which improves the coating's optical and electrical properties while using the same amount of silver.

We also studied the crystallinity of the silver layers incorporated in the low-e coating. To this end, we deposited the same structure as Sample 3 on a substrate and analyzed it by X-ray diffraction. Fig. 3 compares two samples, one with ion treatment on the SnO_x layer prior to deposition of the silver layer and the other without. The silver peak is higher for the sample subjected to the ion treatment, additionally the grain size is 14.8 nm with ion treatment compared to 11.5 nm without treatment, which indicates ion treatment improves the surface properties and promotes greater crystallinity in the silver layer.

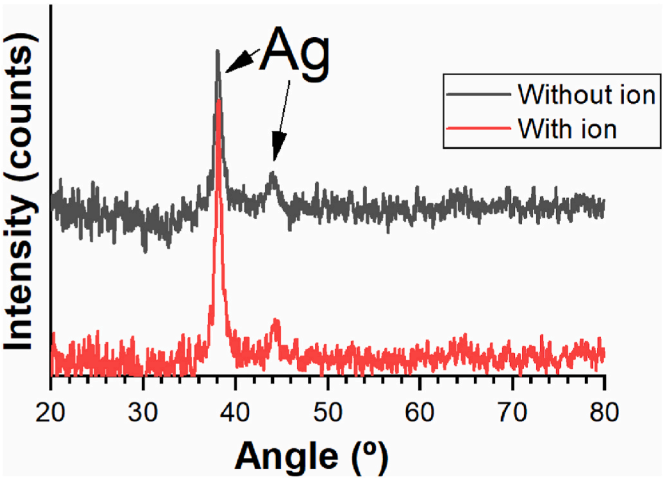

Fig. 3. X-ray diffraction of the Sample 3 structure.

3.3. TEM and EDS

The morphology of the cross-section of Sample 2 has been studied by TEM, Fig. 4. The layer structure can be clearly visualized, the SnO_x layers are clearly observed and have compact morphology and amorphous structure. The intermediate layer of silver is observed and the grains with different orientations of the crystallinity planes can be distinguished with a size according to that obtained by XRD (Additional TEM images are shown in the Supplementary Material, Figures S4(a-d)). The grains are not perfectly isotropic due to the limitation of the thickness of the silver layer as shown in the TEM images. Elemental mapping was performed by EDS, Fig. 5. The elemental distribution clearly corresponds to the layer structure described in Table 2. The mappings of the individual materials are attached in Figure S5 and S6.

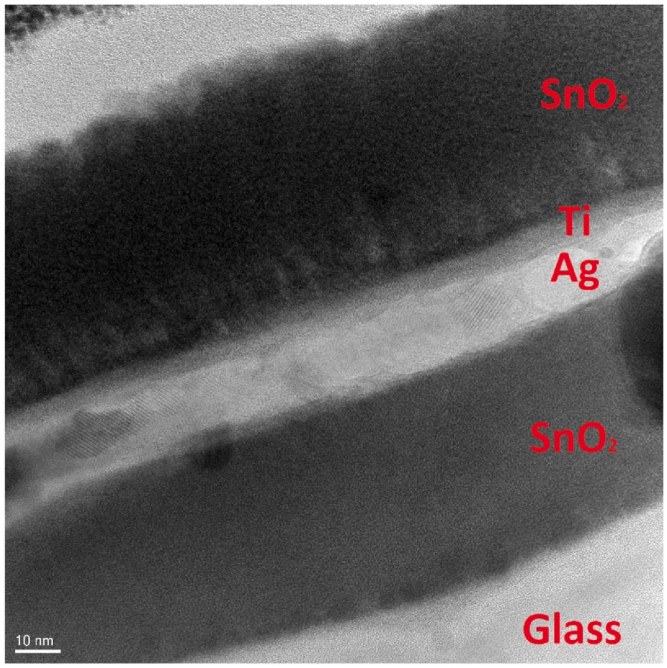

Fig. 4. Cross-section of Sample 2 performed by TEM.

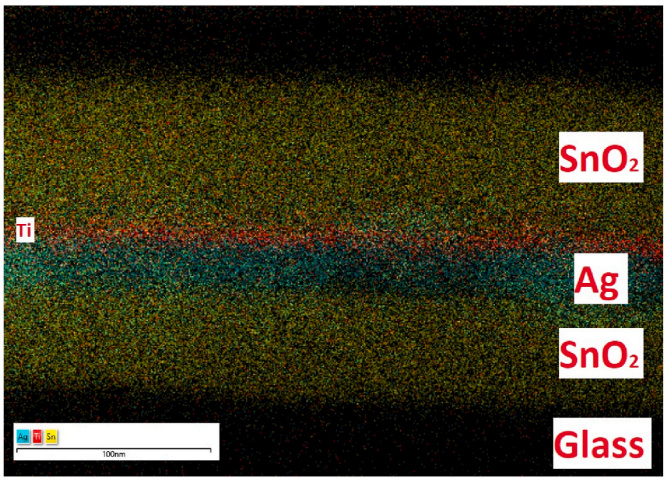

Fig. 5. Elemental mapping of Sample 2 performed by EDS.

(a-e) in the Supplementary Material. A quantification of the chemical composition was performed, obtaining a value of $SnO_{1.91}$, this value is higher than that obtained in other studies of SnO_x layers such as in Refs. [30,31] where values close to x = 1.5 were obtained and slightly larger than [32] where values of x = 1.85 are reported. Our value closest to the stoichiometric value of x = 2 is due to the fact that during the deposition process we used a high flow of O_2 that guaranteed the reactive mode of the deposition. These results guarantee that the SnO_x layer has a high gap value and it is transparent in the visible zone of the spectrum [33–35]. The main contaminants found were sodium (Na), coming from its diffusion from the glass substrate, and carbon (C), which could have its origin in the sample preparation stage for the visualization by TEM (it had to be coated with C for the test). As shown in Figure S6.e, the bombardment of the first layer of SnO_x with Ar ions has not shown an extra implantation of Ar in the coating. The highest concentration of Ar in the coating occurs in the silver layer that was deposited after ion treatment. The concentration of Ar is similar in the first SnO_x layer (deposited before ion treatment) and in the second SnO_x layer (deposited after ion treatment). Finally, the measured concentration of Ar in the SnO_x layers is less than 0.2%. The elemental spectrum and its quantification are shown in Figure S7 of the Supplementary Material.

3.4. Optical properties

We measured the transmittance and reflectance of the structures developed for the study. Fig. 6 shows the spectra obtained for the structure without (Ref) and with the ion gun pretreatment on the SnO_x layers (Ion). It shows the transmittance and reflectance (coating side) in visible and near-infrared, which are the most important parameters for determining the photoenergy properties of the coating. In all cases, the ion treatment produced a slight increase both in transmission in the visible range (380–780 nm) and in reflection in the near-IR (800–2500 nm). These increases improve the coating's photoenergy properties. Obtaining better optical properties using the same amount of silver is a notable achievement, particularly considering the high cost of the silver target used in industrial deposition systems, as it translates into higher

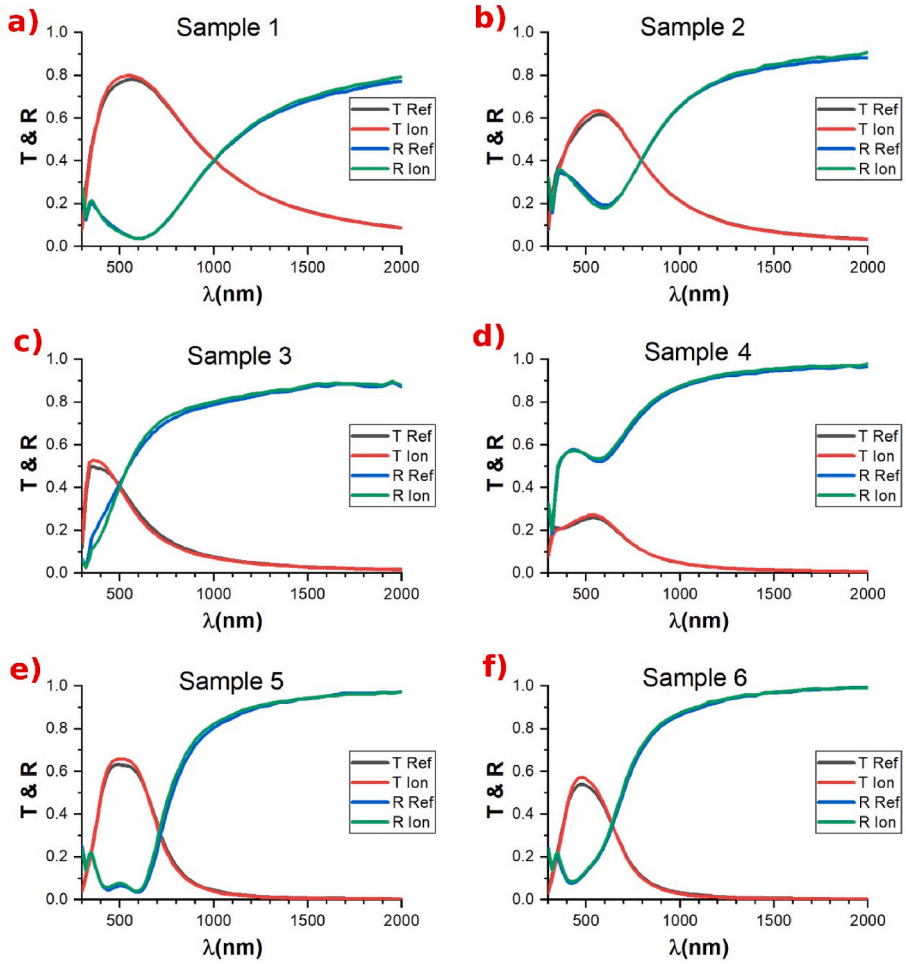

Fig. 6. Transmittance and reflectance (coating side) spectra of the six samples studied.

performance coatings at the same cost.

The same behavior can be observed when comparing the global transmittance and reflectance calculated according to DIN EN410 [36]. Table 6 shows the transmittance and reflectance (solar and visible) on both sides for each of the low-emissivity sample studied, as well as the difference between samples with and without the ion gun pretreatment. Note that the most important parameter of a low-e coating is its visible transmittance, which corresponds to the amount of visible light that can pass through it, and solar reflectance, which indicates the amount of solar energy the coating reflects. The coating is designed to be anti-reflective on the coating side in visible range, hence the importance of compensating for the etching of the SnO_x layer.

As shown in Table 6, the increase in the visible transmittance of samples that received the ion gun pretreatment was between 1.1% and 2.3%, which gives an average increase of approximately 2%. The increase in the total solar reflectance was less evident; as can be seen in the visible region of the spectra (Fig. 6). There was a decrease in reflectance, resulting in a smaller increase in the global solar reflectance despite the clear increase in the near-IR region. The average increase in solar reflectance on the coating side was approximately 0.6%. Thus, we can conclude that the ion gun pretreatment improves the photoenergy properties of low-emissivity coatings.

Fig. 7 and Table 7 show the effects of applying different ion doses. The optimal ion dose was between 0.210 and 0.420 cm/s, since samples 1.3, 1.4, 5.3 and 5.4 had the best photoenergy properties (higher visible transmittance and higher solar reflectance). It should be noted that it is harder to make samples analogous to the references, as the thickness of the layer deposited must be carefully adjusted every time the ion dose is changed.

The increase in visible transmittance with respect to the reference sample was between 2 and 3% of the absolute transmittance, whereas the solar reflectance was barely modified. However, this is a good result considering the improved transmittance (which decreases the visible reflectance).

3.5. Emissivity

Table 8 shows the emissivity for each sample. Note that the emissivity decreases for all samples subject to the ion gun pretreatment. It is important to differentiate between the structures with a single (Samples 1 to 4) or a double layer of silver (Samples 5 and 6). Of those with a single layer of silver, the relative decrease in emissivity was greater for thinner layers of silver. This is because the roughening effect of the SnO_x layer pretreated prior to silver deposition is more pronounced in thinner layers.

The improvement in emissivity was greater at higher ion doses; however, this nominal increase seems to be saturated at high doses, as there was no improvement between samples exposed to doses of 0.210 and 0.105 cm/s.

These results seem to indicate that the best application conditions for the ion treatment are a moderate dose, which equates to a speed of between 0.210 and 0.420 cm/s for the deposition system used here. Higher doses do not improve the quality of the SnO_x surface and may be harder to control in terms of etching, which also means it is harder to control the coating's optical and photoenergy properties. The results obtained for the samples without ion treatment are similar to those obtained in other works such as [13], where an emissivity of 0.09 is obtained for an SnO_x coating with 9 nm of silver. It should be noted that the comparison with other studies is not straightforward because many structures can be manufactured with different thicknesses of silver that affect the values of emissivity, transparency and reflectance. In any case, under similar conditions, results show that the application of the ion treatment improves the photoenergy properties of the coating compared to the samples without ion treatment.

Table 6
Transmittance and reflectance coefficients in both, visible and solar, of the different samples studied.

	Sample 1		Sample 2		Sample 3	
	Ref	Ion	Ref	Ion	Ref	Ion
T_{vis}	77.3%	79.1%	60.4%	62.3%	31.9%	33.5%
R_{vis} (glass side)	11.4%	10.0%	30.8%	29.1%	56.0%	55.8%
R_{vis} (coating side)	5.1%	4.9%	21.6%	20.0%	51.5%	50.9%
T_{solar}	56.4%	57.4%	39.9%	40.5%	22.2%	22.7%
R_{solar} (glass side)	25.3%	24.8%	45.7%	45.6%	67.1%	66.9%
R_{solar} (coating side)	24.0%	24.2%	43.0%	42.8%	61.3%	61.2%
	Sample 4		Sample 5		Sample 6	
	Ref	Ion	Ref	Ion	Ref	Ion
T_{vis}	25.2%	26.3%	60.9%	63.3%	48.2%	50.4%
R_{vis} (glass side)	68.2%	66.4%	6.2%	6.6%	13.5%	16.1%
R_{vis} (coating side)	53.4%	54.5%	5.2%	6.0%	19.7%	20.5%
T_{solar}	14.9%	15.3%	31.6%	32.0%	25.0%	25.5%
R_{solar} (glass side)	74.8%	73.6%	36.6%	37.8%	38.4%	40.0%
R_{solar} (coating side)	69.1%	70.1%	40.2%	41.7%	50.9%	51.9%

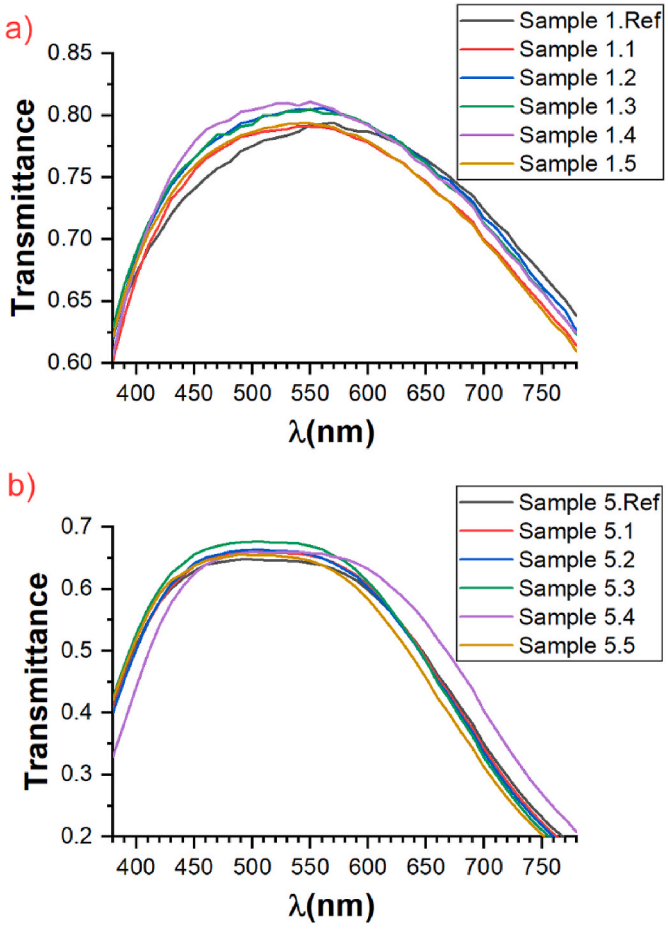

Fig. 7. Visible transmittance spectra as a function of ion dose for Sample 1 (a) and Sample 5 (b).

4. Conclusions

The application of an ion bombardment treatment to SnO_x layers prior to silver deposition in low-e coatings improves the material's photoenergy performance. We have also confirmed that this treatment achieves higher crystallinity in the thin layer of silver deposited in samples subject to the ion pretreatment, this point has been confirmed by XRD and TEM. The main effect of ion bombardment is the

Table 7
Visible and solar (transmittance and reflectance) coefficients in function of ion dose for structures type 1 and 5.

	Sample 1					
	Ref	1.1	1.2	1.3	1.4	1.5
T_{vis}	77.3%	78.3%	79.7%	79.7%	80.1%	78.6%
R_{vis} (glass side)	11.4%	9.4%	9.1%	9.3%	7.7%	8.5%
R_{vis} (coating side)	5.1%	4.1%	4.3%	4.5%	3.9%	3.8%
T_{solar}	56.4%	56.6%	57.8%	57.5%	57.6%	56.7%
R_{solar} (glass side)	25.3%	25.1%	25.4%	25.8%	24.4%	25.1%
R_{solar} (coating side)	24.0%	24.6%	24.6%	25.0%	24.7%	24.7%
	Sample 5					
	Ref	5.1	5.2	5.3	5.4	5.5
T_{vis}	62.5%	63.5%	63.6%	64.8%	64.7%	62.3%
R_{vis} (glass side)	6.3%	6.3%	6.5%	6.3%	8.6%	6.5%
R_{vis} (coating side)	4.8%	5.5%	6.0%	6.0%	8.7%	5.5%
T_{solar}	32.4%	32.4%	32.2%	32.7%	33.3%	31.6%
R_{solar} (glass side)	38.1%	37.8%	37.4%	39.0%	36.8%	38.9%
R_{solar} (coating side)	40.6%	40.5%	41.0%	42.0%	41.4%	41.9%

Table 8
Emissivity for different samples and ion doses. Thickness in samples 5 and 6 stand for the first and the second layer of silver.

Sample	Ag thickness (nm)	Carrier speed (cm/s)	Emissivity without ion (Ref)	Emissivity with ion (Ion)	% improvement
1	10	0.420	0.082	0.071	13.4
2	15	0.420	0.039	0.035	10.3
3	20	0.210	0.026	0.024	7.7
4	27	0.420	0.016	0.015	6.3
5	9 + 14	0.420	0.031	0.027	12.9
6	7 + 19	0.420	0.026	0.022	15.4
1.1	10	1.680	0.082	0.073	11.0
1.2	10	0.840	0.082	0.073	11.0
1.3	10	0.420	0.082	0.069	15.9
1.4	10	0.210	0.082	0.068	17.1
1.5	10	0.105	0.082	0.068	17.1
5.1	9 + 14	1.680	0.031	0.028	9.7
5.2	9 + 14	0.840	0.031	0.028	9.7
5.3	9 + 14	0.420	0.031	0.027	12.9
5.4	9 + 14	0.210	0.031	0.026	16.1
5.5	9 + 14	0.105	0.031	0.026	16.1

morphological change of the surface in the SnO_x layer prior to the deposition of the silver layer, with the appropriate dose of ions, it is possible to reduce the roughness of the SnO_x surface and modify the type of roughness with a smaller bulges size. The ion pretreatment was also shown to enhance the coating's optical properties with increases in visible transmittance of approximately 2% and a slight increase in solar reflectance. This translates into an effective reduction in the amount of silver consumed to produce low-e coatings while retaining their optical properties. Furthermore, this study shows that ion treatment considerably decreases coating emissivity. This improvement is most evident in low-e coatings with thin layers of silver, and we have quantified the effect of different ion doses in order to find the optimal dose.

CRediT authorship contribution statement

E. Carretero: Writing – review & editing, Writing – original draft, Supervision, Methodology, Funding acquisition, Conceptualization. **A. Cueva:** Writing – review & editing, Writing – original draft, Methodology, Investigation. **J. Preciado-Garbayo:** Writing – review & editing. **P. Sevillano:** Writing – review & editing, Software.

Declaration of competing interest

The authors declare the following financial interests/personal relationships which may be considered as potential competing interests: Enrique Carretero reports financial support was provided by Spain Ministry of Science and Innovation. Enrique Carretero reports financial support was provided by Government of Aragon.

Data availability

Data will be made available on request.

Acknowledgements

We gratefully acknowledge financial support from the Spanish Ministerio de Ciencia e Innovación, under the project RTC2019-007368-3 and the "Departamento de Ciencia, Universidad y Sociedad del Conocimiento del Gobierno de Aragón" (group T20_20R). We acknowledge the service from the MiNa Laboratory at IMN, and funding from CM (project S2018/NMT-4291 TEC2SPACE), MINECO (project CSIC13-4E-1794) and EU (FEDER, FSE). Authors acknowledge the use of instrumentation as well as the technical advice provided by the National Facility ELECMI ICTS, node « Laboratorio de Microscopias Avanzadas (LMA)» at « Universidad de Zaragoza». Authors would like to acknowledge the use of Servicio General de Apoyo a la Investigación-SAI, Universidad de Zaragoza. The authors gratefully acknowledge the continued support from the company Ariño Duglass and Catedra Ariño Duglass.

Appendix A. Supplementary data

Supplementary data related to this article can be found at https://doi.org/10.1016/j.vacuum.2022.111485.

References

[1] M. Arbab, Sputter-deposited low-emissivity coatings on glass, MRS Bull. 22 (1997) 27–35, https://doi.org/10.1557/S0883769400033972.
[2] B.P. Jelle, S.E. Kalnaes, T. Gao, Low-emissivity materials for building applications: a state-of-the-art review and future research perspectives, Energy Build. 96 (2015) 329–356, https://doi.org/10.1016/j.enbuild.2015.03.024.
[3] G. Leftheriotis, P. Yianoulis, Characterisation and stability of low-emittance multiple coatings for glazing applications, Sol. Energy Mater. Sol. Cells 58 (1999) 185–197, https://doi.org/10.1016/S0927-0248(98)00202-5.
[4] J. Ebisawa, E. Ando, Solar control coating on glass, Curr. Opin. Solid State Mater. Sci. 3 (1998) 386–390, https://doi.org/10.1016/S1359-0286(98)80049-1.
[5] P. Grosse, R. Hertling, T. Müggenburg, Design of low emissivity systems based on a three-layer coating, J. Non-Cryst. Solids 218 (1997) 38–43, https://doi.org/10.1016/S0022-3093(97)00130-0.
[6] R.J. Martín-Palma, L. Vázquez, J.M. Martínez-Duart, Malats-Riera, Silver-based low-emissivity coatings for architectural windows: optical and structural properties, solar energy materials and solar cells. https://doi.org/10.1016/S0927-0248(98)00007-5, 1998, 53, 55-66.
[7] M.N.-E. Alam, M. Rahman, M.K. Basher, M. Vasiliev, K. Alameh, Optical and chromaticity properties of metal-dielectric composite-based multilayer thin-film structures prepared by RF magnetron sputtering, coatings. https://doi.org/10.3390/coatings10030251, 2020, 10, 251.
[8] J. Mohelnikova, Materials for reflective coatings of window glass applications, Construct. Build. Mater. 23 (2009) 1993–1998, https://doi.org/10.1016/j.conbuildmat.2008.08.033.
[9] G. Ding, C. Clavero, Silver-Based Low-Emissivity Coating Technology for Energy-Saving Window Applications, IntechOpen, 2017, https://doi.org/10.5772/67085.
[10] A. Kloppel, B. Meyer, J. Trube, Influence of substrate temperature and sputtering atmosphere on electrical and optical properties of double silver layer systems, Thin Solid Films 392 (2001) 311–314, https://doi.org/10.1016/S0040-6090(01)01049-5.
[11] B.P. Jelle, A. Hynd, A. Gustavsen, D. Arasteh, H. Goudey, R. Hart, Fenestration of today and tomorrow: a state-of-the-art review and future research opportunities, Sol. Energy Mater. Sol. Cell. 96 (2012) 1–28, https://doi.org/10.1016/j.solmat.2011.08.010.
[12] K. Kato, H. Omoto, T. Tomioka, A. Takamatsu, Visible and near infrared light absorbance of Ag thin films deposited on ZnO under layers by magnetron sputtering, Solar Energy Materials and Solar Cells. https://doi.org/10.1016/j.solmat.2011.04.005, 2011, 95, 2352-2356.
[13] R. Alvarez, J.C. González, J.P. Espinós, A.R. González-Elipe, A. Cueva, F. Villuendas, Growth of silver on ZnO and SnO2 thin films intended for low emissivity applications, Appl. Surf. Sci. 268 (2013) 507–515, https://doi.org/10.1016/j.apsusc.2012.12.156.

[14] M.A. Ruiz-Robles, N.A. bundiz-Cisneros, C.E. Bender-Perez, C.D. Gutierrez-Lazos, A. Fundora-Cruz, F. Solis-Pomar, E. Perez-Tijerina, New ultrathin film heterostructure for low-e application by sputtering technique: a theoretical and experimental study, Mater. Res. Express 5 (2018), 036420, https://doi.org/10.1088/2053-1591/aab6a0.

[15] C. Schaefer, G. Bräuer, J. Szczyrbowski, Low emissivity coatings on architectural glass, Surf. Coating. Technol. 93 (1997) 37–45, https://doi.org/10.1016/S0257-8972(97)00034-0.

[16] Z. Huang, W. Zhou, X. Tang, D. Zhu, F. Luo, Effects of substrate roughness on infrared-emissivity characteristics of Au films deposited on Ni alloy, Thin Solid Films 519 (2011) 3100–3106, https://doi.org/10.1016/j.tsf.2010.12.157.

[17] G. Beister, E. Dietrich, C. Schaefer, M. Scherer, J. Szczyrbowski, Progress in large-area glass coatings by high-rate sputtering, Surface and Coatings Technology. https://doi.org/10.1016/0257-8972(95)02600-2, 1995, 76-77, 776-785.

[18] S.-C. Chang, S.-C. Hung, C.-S. Ye, Y.-J. Hsiao, T.-C. Lin, H.-Z. Cheng, Y.-L. Shen, Thermal stability of SnOx/NiCrOx/Ag/AZO/SnOx/glass multilayer films applied in low-emissivity glass, J. Chin. Soc. Mech. Eng. 39 (2018) 427–431.

[19] M.L. Addonizio, M. Ferrara, A. Castaldo, A. Antonaia, Air-stable low-emissive AlN-Ag based coatings for energy-efficient retrofitting of existing windows, Energy Build. 250 (2021), 111259, https://doi.org/10.1016/j.enbuild.2021.111259.

[20] K. Mizukoshi, T. Yamamura, Y. Tomioka, M. Kawamura, Effect of TiO2 lowermost layer on crystal orientation and electrical resistivity of glass/TiO2/ZnO/Ag structure in Low-E glass, Jpn. J. Appl. Phys. 60 (2021), 025501, https://doi.org/10.35848/1347-4065/abdabd.

[21] K. Sun, X. Tang, C. Yang, D. Jin, Preparation and performance of low-emissivity Al-doped ZnO films for energy-saving glass, Ceram. Int. 44 (2018) 19597–19602, https://doi.org/10.1016/j.ceramint.2018.07.207.

[22] K. Sun, D. Zhang, H. Yin, L. Cheng, H. Yuan, C. Yang, Preparation of AZO/Cu/AZO films with low infrared emissivity, high conductivity and high transmittance by adjusting the AZO layer, Appl. Surf. Sci. 578 (2022), 152051, https://doi.org/10.1016/j.apsusc.2021.152051.

[23] K. Mizukoshi, T. Yamamura, Y. Tomioka, M. Kawamura, Optimization of lowermost layer material for low-resistivity Ag-based multilayer structure in low-emissivity glass, Thin Solid Films 739 (2021), 138996, https://doi.org/10.1016/j.tsf.2021.138996.

[24] M. Yuste, R. Escobar Galindo, S. Carvalho, J.M. Albella, O. Sanchez, Improving the visible transmittance of low-e titanium nitride based coatings for solar thermal applications, Appl. Surf. Sci. 258 (2011) 1784–1788, https://doi.org/10.1016/j.apsusc.2011.10.046.

[25] M.B. Cinali, O.D. Coskun, Optimization of physical properties of sputtered silver films by change of deposition power for low emissivity applications, J. Alloys Compd. 853 (2021), 157073, https://doi.org/10.1016/j.jallcom.2020.157073.

[26] R. Mientus, M. Weise, S. Seeger, R. Heller, K. Ellmer, Electrical and optical properties of amorphous SnO2:Ta films, prepared by DC and RF magnetron sputtering: a systematic study of the influence of the type of the reactive gas, Coatings 10 (2020) 204, https://doi.org/10.3390/coatings10030204.

[27] N.J. Suliali, W.E. Goosen, A.J. van Vuuren, E.J. Olivier, B. Bakhit, H. Hogberg, V. Darakchieva, J.R. Botha, Ti thin films deposited by high-power impulse magnetron sputtering in an industrial system: process parameters for a low surface roughness, Vacuum 195 (2022), 110698, https://doi.org/10.1016/j.vacuum.2021.110698.

[28] Gencoa Ltd., V. Bellido-Gonzalez, J.M. Marco, Ariño-Duglass, I. Sorzabal-Bellido, , Gencoa Ltd., R. Alonso, University of Zaragoza, Effects of Ion Bombardment Pretreatment on Glass Coating Processes and Post Tempering, 2016, pp. 177–181, https://doi.org/10.14332/svc15.proc.1935.

[29] H.J. Glaser, Large Area Glass Coating, Von Ardenne Anlagentechnik, Dresden, 2000.

[30] Q.-H. Wu, J. Song, J. Kang, Q.-F. Dong, S.-T. Wu, S.-G. Sun, Nano-particle thin films of tin oxides, Mater. Lett. 61 (2007) 3679–3684, https://doi.org/10.1016/j.matlet.2006.12.016.

[31] Y. Kim, S.-P. Kim, S.-D. Kim, S.E. Kim, Nitrogen-doped transparent tin oxide thin films deposited by sputtering, Curr. Appl. Phys. 11 (2011) S139, https://doi.org/10.1016/j.cap.2011.03.081. –S142.

[32] F.A. Akgul, C. Gumus, A.O. Er, A.H. Farha, G. Akgul, Y. Ufuktepe, Z. Liu, Structural and electronic properties of SnO2, J. Alloys Compd. 579 (2013) 50–56, https://doi.org/10.1016/j.jallcom.2013.05.057.

[33] S.-S. Lin, Y.-S. Tsai, K.-R. Bai, Structural and physical properties of tin oxide thin films for optoelectronic applications, Appl. Surf. Sci. 380 (2016) 203–209, https://doi.org/10.1016/j.apsusc.2016.01.188.

[34] J.S. Jung, S.J. Park, J.H. Ye, J.G. Woo, B.S. Bae, E.-J. Yun, Optical, structural, and electrical properties of sputter-deposited SnOx thin films, Thin Solid Films 747 (2022), 139139, https://doi.org/10.1016/j.tsf.2022.139139.

[35] Y. Tao, B. Zhu, Y. Yang, J. Wu, X. Shi, The structural, electrical, and optical properties of SnO2 films prepared by reactive magnetron sputtering: influence of substrate temperature and O2 flow rate, Mater. Chem. Phys. 250 (2020), 123129, https://doi.org/10.1016/j.matchemphys.2020.123129.

[36] E. Standards, DIN EN 410. https://Www.En-Standard.Eu. https://www.en-standard.eu/din-en-410-glass-in-building-determination-of-luminous-and-solar-characteristics-of-glazing/.